JGR Space Physics

Key Points:
- Longitudinal expansion of brightening of the substorm onset arc likely represents longitudinal expansion of the substorm onset instability
- Radar flow enhancements with auroral onset longitudinal expansion agree with instability due to longitudinal expansion of intruding bubble
- Westward traveling surge associated with separate flow channel bringing new plasma to field lines head of expansion phase auroral bulge

Radar Observations of Flows Leading to Longitudinal Expansion of Substorm Onset Over Alaska

Larry R. Lyons[1], **Jiang Liu[1,2]**, **Yukitoshi Nishimura[3]**, **Chih-Ping Wang[1]**, **Ashton S. Reimer[4]**, **William A. Bristow[5]**, **Don L. Hampton[5]**, **Xueling Shi[6]**, **Roger H. Varney[4]**, and **Eric F. Donovan[7]**

[1]Department of Atmospheric and Oceanic Sciences, University of California, Los Angeles, CA, USA, [2]Department of Earth, Planetary, and Space Sciences, University of California, Los Angeles, CA, USA, [3]Center for Space Physics and Department of Electrical and Computer Engineering, Boston University, Boston, MA, USA, [4]Center for Geospace Studies, SRI International, Menlo Park, CA, USA, [5]Geophysical Institute, University of Alaska Fairbanks, Fairbanks, AK, USA, [6]Department of Electrical and Computer Engineering, Center for Space Science and Engineering Research, Virginia Tech, Blacksburg, VA, USA, [7]Department of Physics and Astronomy, University of Calgary, Calgary, AB, Canada

Abstract Longitudinal expansion of brightening of the substorm onset arc likely represents longitudinal expansion of the substorm onset instability. We used Poker Flat radar campaign auroral observations to identify seven substorm onsets seen east or west of the radar that expanded into the radar field-of-view. The radar observations were used to show flows relative to the expanding onset aurora. Flow enhancements were found equatorward (poleward) of the westward (eastward) longitudinal expansion of the onset arc brightening that agree with plasma sheet bubble modeling. This lends significant additional supporting evidence that an incoming reduced entropy flow channel leads to onset. As a flow channel enters the auroral oval (plasma sheet) from the polar cap (magnetotail lobes) and starts to move equatorward (earthward in the plasma sheet) as a bubble, it simultaneously expands azimuthally due to the combination of electric drift along dawnward tilted equipotentials and westward magnetic drift of more energetic ions. As the azimuthally expanding bubble reaches near the equatorward boundary of the electron auroral oval, it leads to the onset instability indicated by the auroral beading and associated flows if conditions are appropriate. The instability grows in the initial onset region, as it simultaneously extends longitudinally with the continued azimuthal expansion of the bubble within the plasma sheet. Additionally, after onset, the auroral bulge expands poleward and can lead to a westward traveling surge. We observe strong flows heading toward the front of the surge that appear to bring low entropy plasma, perhaps from the polar cap, into the surge.

1. Introduction

Wave-like modulation of auroral intensity, giving the visual appearance of auroral beads, is the first auroral signature of substorm onset and is the signature of a near-Earth instability initiating the substorm expansion phase (Donovan et al., 2006; Kalmoni et al., 2017; Motoba et al., 2012; Y. Nishimura et al., 2016; Sakaguchi et al., 2009). The onset of beading expands longitudinally within the equatorward portion of the auroral oval (e.g., Shiokawa et al., 2009), this spreading being faster and apparently independent of the later westward (westward traveling surge) and eastward spreading of the auroral bulge (Lyons et al., 2013).

The azimuthal spreading of the beading likely represents longitudinal expansion of the magnetospheric region subject to the onset instability and thus represents an important feature of the onset process, but the azimuthal spreading of substorm expansion phase activity has received only limited attention. S. Zou et al. (2009) found a consistent picture (illustrated in their Figure 14) of electric field and current changes in the ionosphere during substorm expansion phase development as seen from ground-based radars and all-sky imagers (ASIs). West of the initial onset location, enhancement of the SAPS-region electric field was found to occur at latitudes equatorward of the westward traveling surge and with the passing of the surge. These enhancements are within the downward Region 2 field-aligned current (FAC) region. East of onset, eastward flow increases in the region of enhanced downward Region 1 FACs, along with a decrease in ionization and conductivity as expected from the enhanced downward FACs. This flow enhancement decreases

as the auroral bulge expands eastward into the radar field-of-view. Zou and coworkers did not explicitly consider the difference between the azimuthal brightening of the onset arc and the azimuthal expansion of the bulge. Ogasawara et al. (2011) identified events where eastward and westward expansion of expansion phase auroral activity after onset was closely associated with azimuthal flows in the near-Earth plasma sheet that were accompanied by magnetic field dipolarization. However, they did not attempt to distinguish flow channels that lead to onset from those that are common during the ensuing substorm expansion phase (Henderson et al., 1998; Lyons et al., 2012; T. Nishimura et al., 2012; Zhang et al., 2011). Interestingly, Haerendel (2015) suggested that the azimuthal spreading (eastward directed in the case discussed) of onset activity along a breakup auroral arc might be related to an azimuthal directed flow connected with an adjacent streamer, though the paper did not propose an idea of how the connection might arise.

As discussed in the companion paper (Lyons et al., 2021), radar observations show quite clear evidence that the intrusion of lower-entropy plasma (than that of the surrounding plasma) via a plasma sheet flow channel leads to the instability onset as proposed using auroral observations by Y. Nishimura et al. (2010a, 2010b). The goal of the present paper is to evaluate whether longitudinal expansion of the reduced entropy plasma due to magnetic drift as seen in Rice Convection Model (RCM) modeling (Wang et al., 2018; Yang et al., 2014) has observable features consistent with such expansion being responsible for the longitudinal expansion of the onset instability. This would add significant support to the proposal that substorm onset is the result of an instability initiated by the intrusion of a low-entropy flow channel to the onset location.

Multispacecraft observations in the tail suggested that most low-entropy plasma bubbles expand longitudinally when they move earthward to the near-Earth region (Liu et al., 2015; JA020997), but it is unclear from this study whether and how these expanding bubbles can impact substorm onset or development. This is because in situ tail observations alone cannot provide a global view of processes in the magnetosphere and ionosphere. However, by taking advantage of RCM modeled structuring of plasma sheet flows and their response to an intruding low-entropy plasma bubble, we can use radar and optical observations of the ionosphere to test for, and examine the effects of, longitudinal expansion of intruding low entropy plasma. As discussed in Liu et al. (2020), the nightside auroral oval and plasma sheet can have both the well-known subauroral polarization stream (SAPS) region and an analogous dawnside polarization stream (DAPS) region. Both are believed to be associated with enhanced large-scale convection and with plasma sheet flow bursts. SAPS consist of strong westward flows in the low conductivity region of downward Region 2 field-aligned currents (FACs) that lies just equatorward of the electron auroral oval. DAPS consist of strong eastward flows in the poleward, downward Region 1 FAC (poleward) portion of the dawnside auroral oval, where auroral precipitation (Lyons & Fennell, 1986; S. Zou et al., 2009) and thus conductivities are much lower than within the more equatorward, upward Region 2 FAC portion of the auroral oval.

Self-consistent simulations of Wang et al. (2018), described in Section 2, show that both the SAPS and DAPS regions can be enhanced due to enhancement of FACs associated with the earthward (equatorward in the ionosphere) moving flow channels that are consistent with the observations of S. Zou et al. (2009). In Section 3, we use ground-based Poker Flat Incoherent scatter radar (PFISR) and Super Dual Auroral Radar Network (SuperDARN) observations and Poker Flat and THEMIS ASI observations as in the companion paper. We apply these observations to the eastward and westward expansion of substorm onsets by identifying onsets during the PFISR Ion Neutral Observations in the Thermosphere (PINOT) (Makarevich & Bristow, 2014) campaign that are near but west of and east of, respectively, the PFISR radar field-of-view (FOV). As in the companion paper, we analyze all the detected onsets, including the onsets that expanded poleward to a full substorm and those with limited poleward expansion (i.e., pseudo-substorms). While they are not all isolated substorms, they are not a rebrightening of preceding activity but a clean onset that is separate from preceding activity. To the extent feasible, we identify responses that are likely due to preonset flow channels, though both pre- and postonset flow channels can lead to DAPS and SAPS responses could contribute to longitudinal expansion of the instability that gives beading of the onset arc.

2. RCM-UCLA Modeling of a Plasma Bubble

To illustrate the plasma sheet response to an incoming plasma bubble during substorm growth phase conditions, Figure 1 shows results in the equatorial plane using the UCLA equilibrium version of the RCM-UCLA of Wang et al. (2018) for times 3, 9, and 15 min after a mesoscale perturbation with a 1 h in MLT width
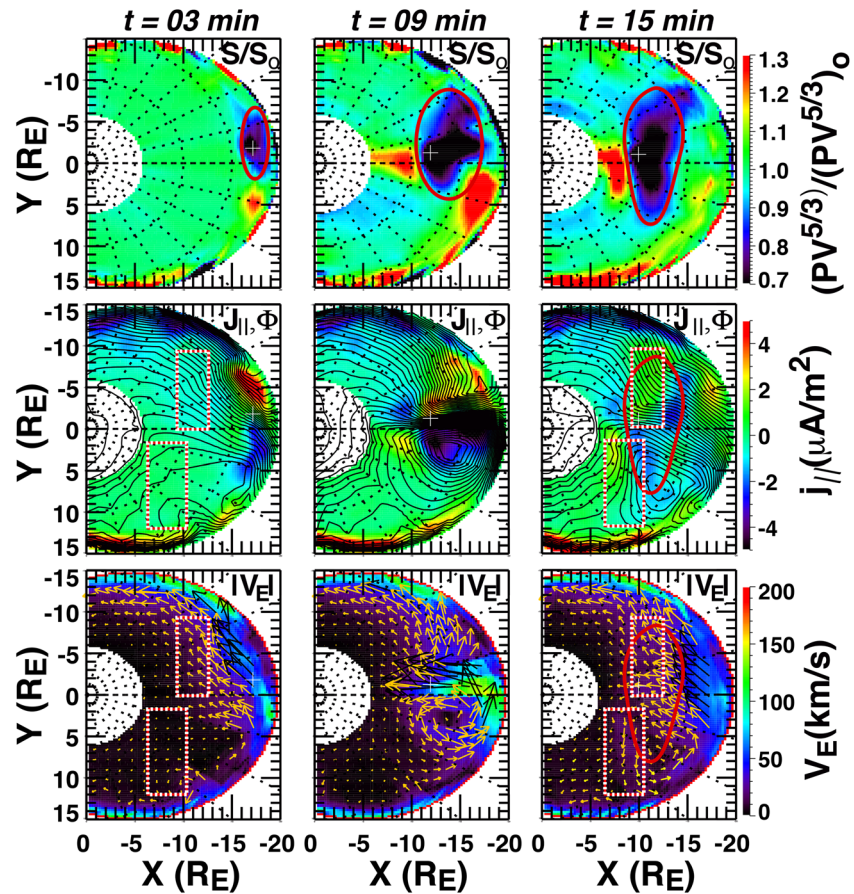
Figure 1. Nightside RCM-UCLA results of Wang et al. (2018) for times 3, 9, and 15 min after a mesoscale perturbation with a 1 h in MLT width was imposed on the RCM outer boundary that lead to bubble formation from energy-dependent magnetic drift. The top row shows the ratio of flux tube integrated entropy S to the integrated entropy S_o at $t = 0$. The middle row show field-aligned current density at the top of the ionosphere and equipotential contours with 2 kV separation, and the lower row should the electric field drift speed both color coded and as vectors. Crimson curves in the top row illustrate the approximate boundary of the expanding bubble for each of the three times, and the crimson curve from the top row at $t = 15$ min is copied onto the middle and lower rows. Red and white rectangles are drawn to help identify the locations for making the comparison between equipotentials and electric field drifts at $t = 3$ and $t = 15$ min. RCM, Rice Convection Model.

was imposed on the RCM outer boundary, which is near $X = -20$ R_E at midnight. A cross-polar cap potential drop of 90 keV was used, which is reasonable for a substorm growth phase. The RCM allows for the energy dependent magnetic drift of isotropic ions and electrons of different energies, and thus allows for bubble evolution via divergence of the heat flux vector, and the UCLA-RCM, incorporates the original RCM with separately developed observation-based tail particle boundary conditions (Wang et al., 2011), force-balanced magnetic field (Gkioulidou et al., 2011), and observation-based electron loss rates (Gkioulidou et al., 2012).

Since the perturbation (Run 1 of Wang and coworkers) had a density decrease by a factor of 6 and a temperature increase by a factor of 6, the bubble was created by the divergence of the heat flux vector resulting from the higher magnetic drift speeds of the hotter plasma particles relative to those of the cooler background. As the bubble moves earthward, the lower energy ions tend to follow the electric field drift (along equipotentials, which are shown as the black contours in the middle row), while the higher energy ions magnetic drift toward the duskside. As a result, the bubble grows by spreading in longitude as it moves earthward. The spreading can very clearly be seen in the top of Figure 1 which shows the ratio of flux tube integrated entropy S to the integrated entropy S_o at $t = 0$ ($S = PV^{5/3}$, where P is plasma pressure and V is flux tube volume). A crimson curve illustrated the approximate boundary of the expanding bubble for each of the

three times. S typically has a tailward gradient in the plasma sheet. However, the bubble spreading leads to an approximately azimuthal-aligned decrease in the tailward gradient in S at $t = 15$ min, a gradient change that could be important (e.g., Xing & Wolf, 2007) for azimuthal expansion of the substorm onset instability.

As can be seen in the middle row of Figure 1, the bubble is associated with enhancement of the Region 1 and 2-sense FACs as it moves earthward ($t = 9$ min), and these FACs become longitudinally broad Region 1 and Region 2-sense currents as the bubble spreads substantially in azimuth after approaching the subauroral region ($t = 15$ min). The enhanced Region 1-sense FACs at $t = 15$ min are approximately collocated with the bubble itself (crimson curve from the top row at $t = 15$ min is copied onto the middle and lower rows of Figure 1), whereas the enhanced Region 2 FACs are earthward of the bubble (There are additional more poleward FAC changes at $t = 15$ min that we do not consider here).

Associated with the enhanced FACs are changes in the electric field, as is required for maintaining current continuity in the ionosphere. The electric changes appear as azimuthal turnings of the flows as the flow channel moves earthward ($t = 9$ min) toward the inner plasma sheet. By $t = 15$ min, this corresponds to significant enhancements in the SAPS and DAPS flows in the regions of the enhanced downward FACs, where conductivities are substantially lower than in the upward FAC regions. These enhancements can be seen by comparing the electric equipotentials and the electric field drift velocities in the middle and bottom rows, respectively, at $t = 3$ and $t = 15$ min. Red and white rectangles in Figure 1 are drawn to help identify the locations for making this comparison, and comparison with the crimson curve shows that the DAPS increase in within the plasma sheet bubble, while the SAPS increases are adjacent to the equatorward boundary of the bubble.

The azimuthal turning of the flows in the plasma sheet at $t = 9$ min is similar to that seen by Ogasawara et al. (2011) within the plasma sheet during substorm azimuthal expansion and offers an explanation for the connection between azimuthal flows and adjacent streamers as suggested by Haerendel (2015), and the current and flow enhancements at $t = 15$ min are very much like those seen from the ground by S. Zou et al. (2009) during the azimuthal development of the substorm expansion phase. These correspondences indicate the plausibility that azimuthal expansion of the substorm onset instability is related to the expansion of incoming reduced entropy bubbles. Note that the azimuthal spreading and associated azimuthal flows of a bubble result from the energy-dependent drift in the RCM. Since this is not included in MHD, the spreading and flows are beyond the capabilities of current MHD simulations of bubbles (e.g., Birn et al., 2004).

3. Observations

Since the electric potentials associated with a bubble give current continuity and map from the magnetosphere to the ionosphere, bubble-related electric field enhancements within the ionosphere have the potential to be used of a signature of the longitudinal expansion of bubble. For example, ground radar observations have previously shown SAPS enhancements following auroral streamers and their associated flow channels in the absence of substorms (Gallardo-Lacourt et al., 2017; Lyons et al., 2015; Makarevich et al., 2011), and DAPS enhancements can be inferred from the connection of the formation of dawnside, auroral omega bands to aurora streamers (Henderson et al., 2002) and to strong DAPS flows (Liu et al., 2018). To illustrate the capability of seeing the azimuthal turning of flow channels with PFISR, Figure 2 shows a sequence of Poker Flat 557.7 nm auroral images overlaid with LOS flows measured by PFISR. This auroral sequence starts with an intensified arc along or near the auroral poleward boundary that subsequently turns equatorward as a streamer and approaches the equatorward portion of the auroral oval. As marked by yellow arrows, the enhanced flow associated with the streamer is seen first (0926:35 and 0927:40 UT panels). Subsequently westward and eastward flow enhancements can be seen toward the west and east, respectively, of the streamer, the westward flow enhancement being equatorward of an auroral enhancement (upward FAC) that turns toward the west (seen most clearly in the 0936:20 UT panel) and the eastward flow being poleward of an auroral enhancement that turns toward the east (0931:34 and 0940:27 UT panels).

Using the ASI and radar data as described in Section 2 of the companion paper, we now consider onsets observed near, but west of and east of the PFISR radar FOV.
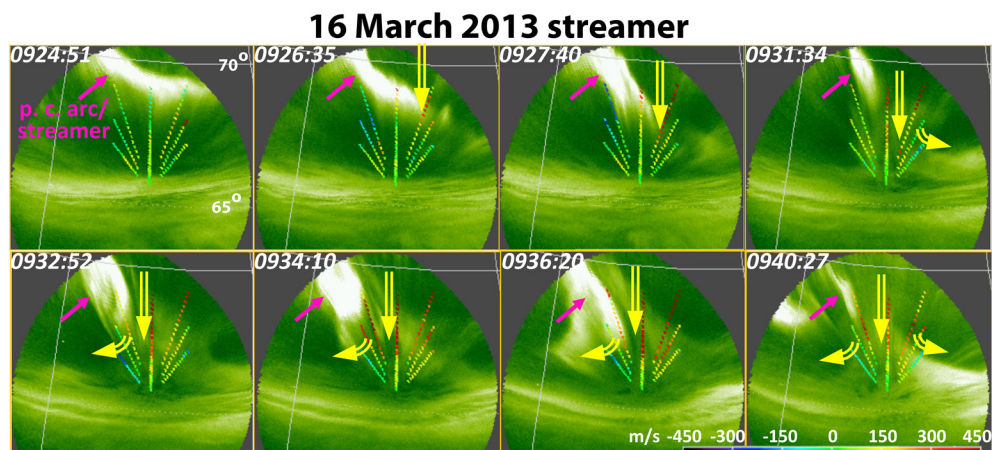
Figure 2. A sequence of Poker Flat 557.7 nm auroral images on March 16, 2013 overlaid with LOS flows measured by PFISR. An auroral arc along or near the auroral poleward boundary that subsequently turns equatorward as a streamer is identified, and yellow arrows mark the enhanced flow associated with the streamer. PFISR, Poker Flat Incoherent scatter radar.

3.1. Events 1 and 2: November 17, 2012, 1058:20 and 1116:40 UT West of FOV Onsets

Figure 3 shows auroral and radar observations for two onsets on November 17, 2012 that were about 18 min apart and were within the western portion of the 557.7 images and distinctly west of the PFISR FOV (see caption for description). Additional File S1 (which gives ground magnetometer data for all eight events considered here) shows small ~30–60 nT ground magnetic north N component drops for both events. Both showed a few degrees of auroral poleward expansion, so we view these as small full substorm onsets. Additional File S2 shows a three-panel movie with full time resolution images (every ~12 s) (The left and center panels of S2, respectively, show 557.7 nm images overlaid with the PFISR LOS velocities along radar beams and the PFISR flow vectors and SuperDARN LOS velocities. The right panels show 630 nm images overlaid with PFISR plasma densities along the radar beams. Radar observations in S2 are stepped in time with the appropriate radar time resolution).

Eastward flow can be seen in both the LOS and vector PFISR flows soon after the first onset. There flows increased substantially as the onset expanded eastward, as can be seen by the LOS flows at 1105:12 and 1106:27 UT and the corresponding vectors at 1105:50 and 1106:52 UT. Furthermore, this flow enhancement was adjacent to and poleward of the brightening arc, consistent with being within the DAPS region of downward FAC on the dawnside. Since the aurora has expanded poleward and streamers had started to appear within the bulge by the time the DAPS flow enhancement was observed, the flow enhancement might have been from the preonset flow channel or a streamer related flow channel during the early expansion phase. The DAPS flow decreased as the activity with the first onset subsided, as can be seen in the first two rows of the lower portion of the Figure 3. Then, as can be seen in the subsequent panels, the DAPS flows increased substantially following the second onset and its eastward expansion. For this onset, the DAPS increase was observed just as the beading was first detected to the west and started to move eastward toward the PFISR FOV, so the increase is likely from the expansion of the bubble that led to the onset.

Also, as seen with several of the events in the companion paper, the 630 nm images in Figure 3 show a streamer, which indicates there was a flow channel coming in toward the location of the initial brightening of the first onset. There is also evidence of a polar cap patch heading toward the location where the streamer formed. Based on Y. Zou et al. (2015), this is additional evidence for a flow channel and that it came from the polar cap and lead to the preonset streamer. For this event, there is also a very clear polar cap arc (identified as a polar cap arc because it extended well poleward of the main observed auroral oval) that moved westward with time. We illustrate this motion by including 630 nm images for earlier times than we do for the 557.7 nm emissions in Figure 3. This arc shows that a polar cap flow channel moved westward in time until it reached the location of the second onset at the time of that onset, indicating that this flow channel led to the onset and the ensuing eastward expansion and its associated DAPS increase.
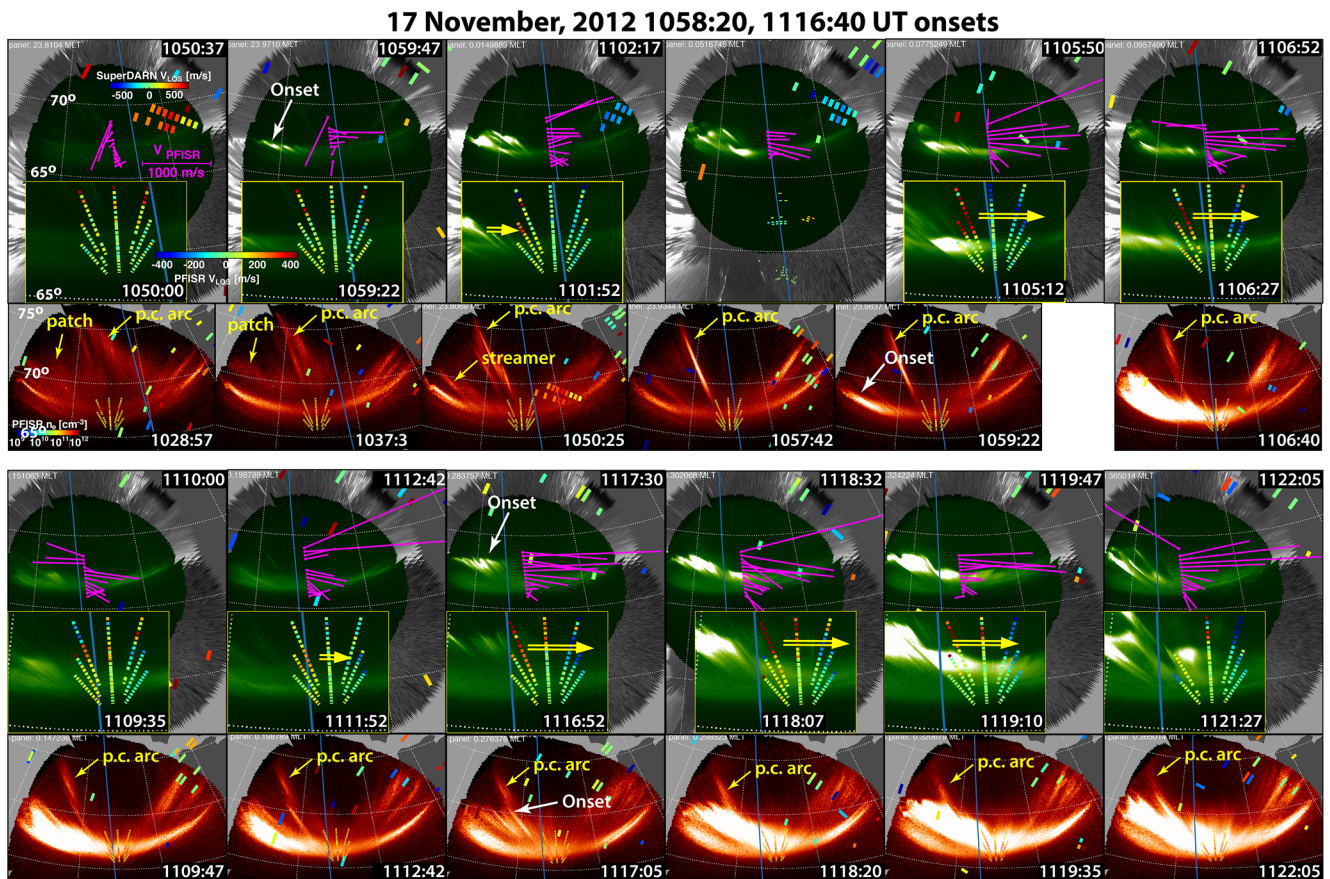
Figure 3. The upper panels of each row show 557.7 nm images from Poker Flat, with THEMIS ASI image mosaics for the region surrounding the Poker image FOV for events 1 and 2, the 1058:20 and 1116:40 UT onsets on November 17, 2012. Images are show at times selected to illustrate features of interest. Objective flow vectors of Heinselman and Nicolls (2008) as a function of latitude along the PFISR magnetic meridian are overlaid on the 557.7 images in each panel. LOS flows measured along the radar beams are shown overlaid on the lower image inserted into each of the 557.7 panels. These lower images are blowups of the 557.7 nm images over the region covered by the PFISR beams, and, to not repeat images, which have 12 s time resolution, these images are for a slightly earlier time than the time of the full mosaics but during the same 1 min of PFISR signal integration. The lower panels of each row show a sequence Poker 630 nm images for this event. In case a reader might be interested, the plasma densities along each radar beam are overlaid of the images. LOS flows from available SuperDARN radar echoes are shown in the 5,577 and 630 nm images panels, the spatial extend of the coverage shown being larger in the 630 nm panels because of the larger spatial FOV of the 630 nm images due to their higher emission altitude (taken to be 110 km for the 557.7 nm and 230 km for the 630.0 nm). The echoes are along radar beams that fan out with distance from the radars, which are located equatorward of the observed auroral oval. Yellow arrows in the 557.7 nm insert are to illustrate flow directions inferred from the PFISR LOS flows, substorm auroral onset is identified by white arrows, and yellow arrows in the 630 nm panels identify an equatorward moving polar cap patch. Magnetic midnight meridian is shown by a blue line in the panels. PFISR, Poker Flat Incoherent scatter radar.

3.2. Events 3, 4, and 5: March 14, 2013, 0938:20 and 0949:22 UT; March 15, 2013, 1051:15 UT West of FOV Onsets

On March 14, 2013 (Figure 4), there was a pseudo-substorm having very little magnetic perturbation that was followed in 11 min by a full substorm with measured N decreases of almost 200 nT. Additional File S3 shows the three-panel movie with full time resolution images. The 630.0 nm images show a clear polar cap arc that indicates a flow channel approaching the time and location of the pseudo-substorm onset. For this event, there were SuperDARN echoes in the region just equatorward of the equatorward boundary of detectable aurora just to the west of the polar cap arc. This is likely the SAPS region. An increase in these flows (darker blue colors at 0938:57UT in Figure 4 and at 0940:00 in S3) can be seen, indicating a SAPS increase consistent with the impact of a flow channel leading to the onset and its expansion to the west. As the onset spread eastward, PFISR saw LOS flows along the beam directed to the west of magnetic north (see 0940:37 UT panel in Figure 4 and S3) that are consistent with equatorward or eastward flows from the incident plasma bubble. As seen in S3, both of these flows soon decreased as did the auroral activity. Then a
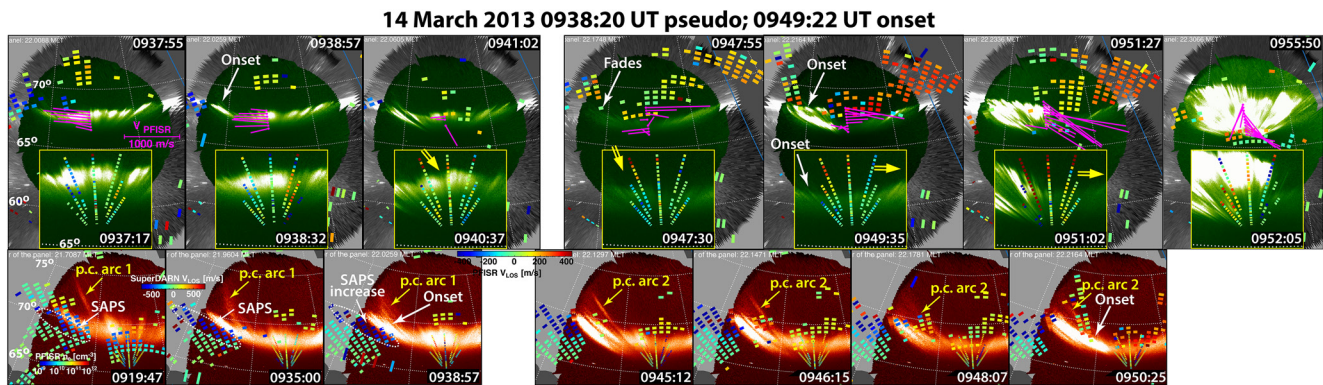
14 March 2013 0938:20 UT pseudo; 0949:22 UT onset

Figure 4. Observations from events 3 and 4, the March 14, 2013, 0938:20 and 0949:22 onsets, in the same format as Figure 3.

new polar cap arc or streamer appeared at ~0943:20 UT, indicating a flow channel approaching to the time and location of the second onset. The DAPS region flows became eastward and strongly increased as the auroral activity expanded eastward to the PFISR FOV. As can be seen in S3, this DAPS increase was first seen at ~0950:00, before significant poleward expansion of the aurora indicating that this increase resulted from the preonset streamer and not an ensuing streamer during the early expansion. The DAPS increase for the pseudo substorm was also likely from the preonset streamer since there was not significant auroral poleward expansion.

The onset on March 15, 2013 (Figure 5, Additional File S4) lead to a full substorm with almost 300 nT N decrease. This is a remarkable event in that all the flow features discussed here can be seen. The incoming flow channel leading to the onset was seen by SuperDARN adjacent to a polar cap arc, as identified in the 1043:45 and 1050: 25 UT 630 nm panels of Figure 5. SuperDARN also shows very clearly a flow increase that is likely SAPS, since it is equatorward of detectable aurora. The increase is seen after onset but before auroral poleward expansion, and thus it is likely associated with the preonset flow channel that led to onset. Additionally, an increase in DAPS flows as onset spread eastward into the PFISR FOV can be seen in both the LOS and vectors flows in the final two 557.7 panels of Figure 5, and this increase also was first seen before significant auroral poleward expansion (While not directly relevant to the current paper, there is a sharp transition to westward flows at the poleward boundary of the DAPS flows. This possibly corresponds to the auroral poleward boundary, and the more poleward SuperDARN LOS flows are consistent with flows being westward within the nearby polar cap).

For all five of the above events, the PFISR observations show an enhancement of the DAPS flows as the onset auroral activity spread eastward to the FOV of PFISR, showing marked consistency with onset resulting from a plasma sheet bubble and eastward expansion of the bubble being responsible for the eastward expansion of the onset instability. For four of these five events, the DAPS increase was first seen before significant auroral poleward expansion, consistent with it being associated with the bubble responsible for onset. For
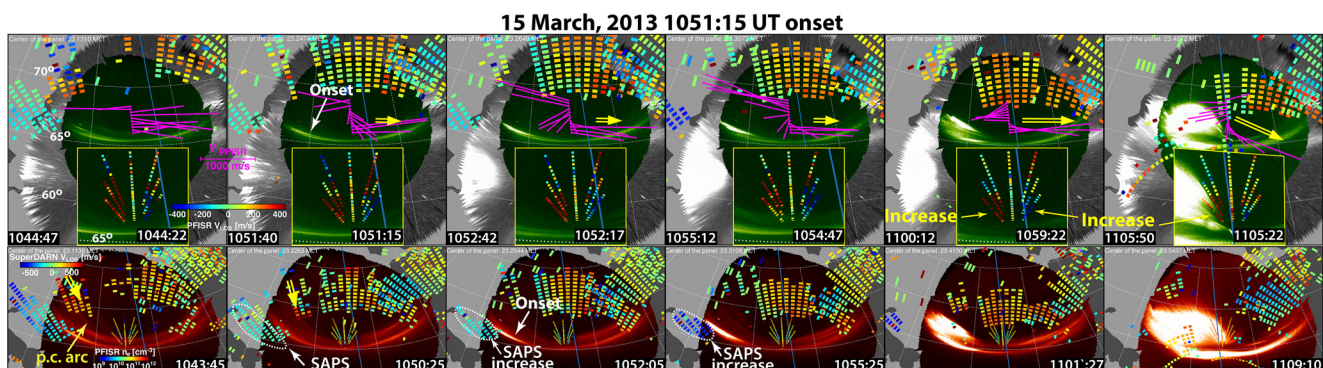
15 March, 2013 1051:15 UT onset

Figure 5. Observations from event 5, the March 15, 2013, 1051:15 onset, in the same format as Figure 3.
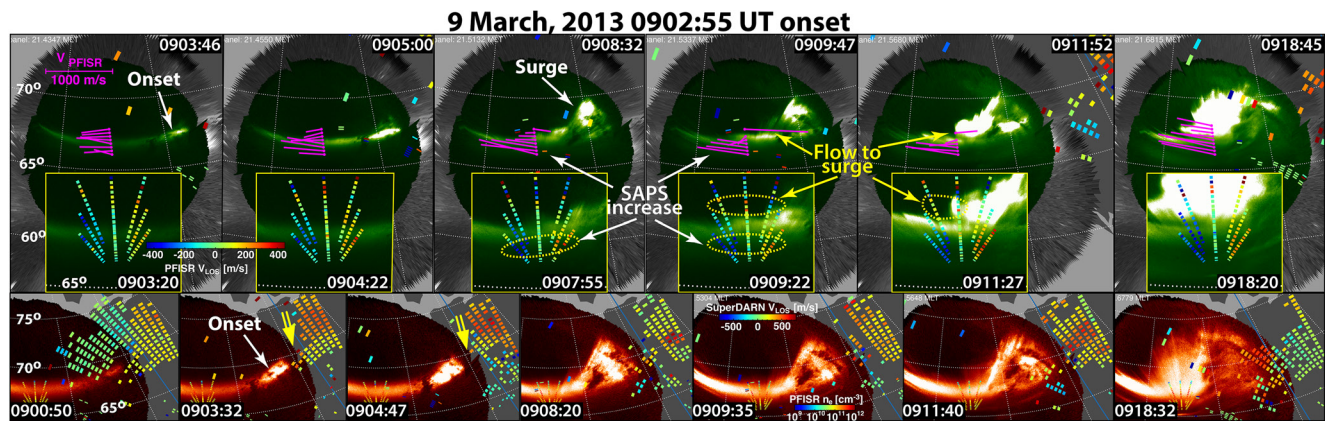
Figure 6. Observations from event 6, the March 9, 2013, 0902:55 onset, in the same format as Figure 2.

two of the events, the availability of SuperDARN echoes allowed to also see the SAPS flow increase to the west of the incoming flow channel, and before significant auroral expansion, as the model results in Figure 1 show to be the result of westward expansion of a bubble by magnetic drift.

3.3. Event 6: March 9, 2013, 0902:55 UT East of FOV Onset

The event with onset at 0902:55 UT on March 9, 2013 (Figure 6, Additional File S5) is the only event we have with onset east of PFISR and also within the latitude range of the PFISR FOV but at high enough latitude for PFISR to see the SAPS response as the onset expanded westward. Onset is identified in the first 555.7 nm and the second 630 nm panels of Figure 6. This was a moderately strong full substorm with N decrease of almost 400 nT. As indicated in the second and third 630 nm panels, SuperDARN appears to have seen the incoming flow channel that lead to the onset. Westward SAPS flow can be seen prior to and just following the onset, consistent with substorm growth phase convection. Then, as the onset auroral brightening spread westward and entered the PFISR FOV (third and fourth 555.7 nm panels), both the LOS flows and the flow vectors show an increase in the SAPS flows of (based on the vectors) ~200 m/s. Since a few degrees of auroral poleward expansion has occurred before the SAPS flow increase was first seen, the SAPS increase could have been to an early expansion phase flow channel or the one that led to onset.

Also seen with the 557.7 nm images for this event is the oncoming westward traveling surge, which is a separate feature of substorm expansion. The surge initiates later than does the longitudinal expansion of the brightening of the onset arc, and typically develops after auroral activity reaches the polar cap boundary and then protrudes into the preexisting polar cap (Lyons et al., 2013). Lyons and coworkers saw a continuing connection between an arc along the auroral poleward boundary arc and the front of the westward traveling surge, suggesting that the surge appears to be fed by plasma from the polar cap that flows adjacent to the poleward boundary arc and toward the front of the westward traveling surge. However, the available data did not allow for direct observations of the incoming flows. On the other hand, for this event as seen in Figure 6, the PFISR observations show direct evidence for such flows. They are seen in both the LOS and vector flows as eastward flow poleward of the brightened aurora to the west of the surge (0909:47 and 0911:52 UT panels and their 0909:22 and 0911:40 UT inserts), giving two distinct flow regions. The flows toward the surge are no longer visible once the surge moves westward across the PFISR FOV.

3.4. Event 7: November 24, 2012, 0545:30 UT East of FOV Onset

The onset in Figure 7 (Additional File S6) occurred very near the eastern edge of the 557.7 nm images and westward traveling surge formation is first clearly seen in the 0556:02 UT image of S6. This was a moderately strong full substorm with N decrease of almost 500 nT. As can be seen in the PFISR LOS flows in the inserts of Figure 7, PFISR was running with many more beams than for our previous events. Despite the reduced total radar time for each beam, we are fortunate that the LOS flows using 1 min time integration times are no noisier than for the previous events, allowing for substantially better spatial resolution. The
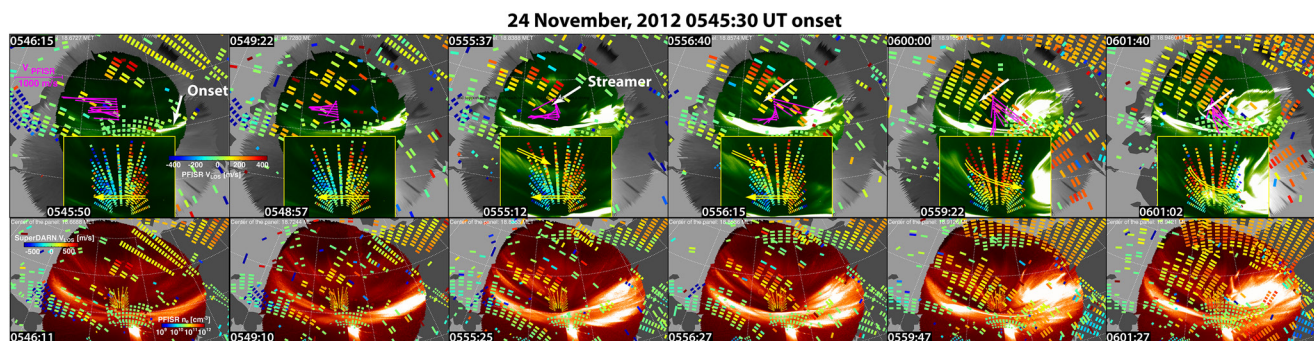
24 November, 2012 0545:30 UT onset

Figure 7. Observations from event 7, the November 24, 2012, 9545:30 onset, in the same format as Figure 2, except the 630 nm images are not included.

onset arc was about 1° equatorward of the PFISR FOV, so SAPS flow cannot be observed. However, westward flows were seen poleward of the onset arc prior to onset. There flows were likely weaker than the SAPS flows, as can be seen for the event in Figure 6.

A streamer is identified in the 0555:37 UT and subsequent 557.7 nm images in Figure. It is first discernible at 0552:05 UT in S6. As seen during the events in Lyons et al. (2013), the eastern portion of this streamer dipped equatorward as the surge approached. Once the streamer entered the PFISR FOV, the vector flows (0556:40 UT panel) and LOS flows (0556:15 UT insert) show strong, approximately southeastward directed, flows poleward of the streamer. The streamer and the southeastward flows continued to dip equatorward as the surge approached, and the flows were continuously directed toward the head of the oncoming surge. Notice the blue colored flow measurement points (away from the radar) in the eastern looking beams in the 0601:02 UT insert. These points are as close to the front of the oncoming surge as can be discerned with the measurement time and spatial resolution, consistent with these flows bringing low-entropy plasma into the surge. It is also interesting that SuperDARN also saw strong LOS flows (bottom row of Figure 6) that are consistent with the flow vectors directed toward the surge seen by PFISR, and the strongest flows (deep orange colored data points) moved westward with the surge. That these flows are seen beyond 75° magnetic latitude suggest a direct connection between the flows impinging on the front of the surge and flow structures within the polar cap. Such flows could directly bring lobe plasma to the head of the surge or might lead to a bubble on closed field lines that carries reduced entropy plasma into the surge.

4. Summary and Conclusions

In the companion paper, we used radar observations over Alaska to provide evidence that low entropy plasma from intruding flow channels leads to the majority of substorm onsets as initially proposed by Y. Nishimura et al. (2010a). We suggested that the reduced entropy of this new plasma relative to that of the surrounding plasma gives rise to a substorm onset instability that is manifested as the growing auroral and electromagnetic waves seen with substorm auroral onset. If correct, this explanation must also account for the observed longitudinal spreading with time of the onset of auroral beading and brightening within the equatorward portion of the auroral oval. In this study, we have evaluated this proposal for the longitudinal spreading by using the plasma sheet flows response to an intruding low-entropy plasma bubble predicted by the RCM and seen in previous observations. We used PFISR and SuperDARN observations of ionospheric flows and Poker Flat and THEMIS ASI observations of the aurora, as in the companion paper, and we have selected substorm onsets (listed with observed features in Table 1) seen in the auroral images near but east of or west of the PFISR radar FOV that expanded westward and eastward, respectively, into the PFISR FOV.

We identified five onsets initiating west of the PFISR FOV during the PINOT campaign. For each of these events, the PFISR observations show an enhancement of the DAPS flows (poleward of the main zone of dawnside aurora) as the onset auroral activity spread eastward to the FOV of PFISR.

For two of the events, SuperDARN echoes were available that allowed to also see the SAPS region (equatorward of the duskside electron aurora) west of the inferred location of the incoming flow channel, and these observations showed flow increases that are likely in the SAPS region. We also identified an event

Table 1
Events With Features Observed and by What Instrument or Auroral Feature

Date	Onset UT	Relative location	Onset flow channel	DAPS increase	SAPS increase	Flow to surge
Nov 17, 2012	1058:20	West	Streamer	PFISR	–	–
Nov 17, 2012	1116:40	West	p.c. arc	PFISR	–	–
Mar 14, 2013	0938:20	West	p.c. arc	PFISR	S-darn	–
Mar 14, 2013	0949:22	West	p.c. arc	PFISR	–	–
Mar 15, 2013	1051:15	West	p.c. arc, S-darn	PFISR	S-darn	–
Mar 9, 2013	0902:55	East	S-darn	–	PFISR	PFISR
Nov 24, 2012	0545:30	East	–	–	–	Streamer, PFISR

Note. Location is relative to PFISR meridian where 24 MLT occurs at 1105 UT, p.c. = polar cap, S-darn = SuperDARN.

with onset to the east of the FOV of PFISR that allowed for the detection by PFISR of SAPS flows, and the PFISR observations for this event also showed an increase in the SAPS flows as the onset auroral brightening spread westward.

The observations for all the above 6 identified onsets during the PINOT campaign are consistent with the RCM-UCLA model results in Figure 1 for the azimuthal expansion of a flow channel. Furthermore, in addition to the direct measurements of the flow channels leading to onset in the companion paper, we also see evidence of these onset flows for each of the above six events, one being seen by SuperDARN and also inferred by an auroral streamer or polar cap arc, one being seen with only the SuperDARN flows, and four being inferred by only an auroral streamer or polar cap arc signature. The direct measurement and auroral inference of the flows leading to the time and location of onset in both papers gives by itself strong support for the proposal that the incoming reduced entropy flow channel leads to onset via an intruding low-entropy flow channel, and the observations of the DAPS and SAPS flow enhancement associated with the onset longitudinal expansion lend additional supporting evidence.

Figure 8 schematically summarizes the scenario for substorm onset that we are proposing and that is supported by the data discussed in this and the companion paper, as well as in previous papers referenced earlier. The background convection (dotted and dashed lines) is based on the earlier RCM-UCLA simulations of large-scale convection of Gkioulidou et al. (2009). The top panel shows a flow channel entering the auroral oval (plasma sheet) from the polar cap (magnetotail lobes), where it gives rise to an auroral poleward boundary intensification (PBI). It starts to expand azimuthally as it moves equatorward (earthward in the plasma sheet) due to the combination of electric drift along dawnward tilted equipotentials and westward magnetic drift of the more energetic ions. As shown in the middle panel, when the azimuthally expanding bubble reaches to near the equatorward boundary of the electron auroral oval, the instability indicated by the auroral beading and its associated flows is initiated if conditions are appropriate. As the instability grows (lower panel), auroral activity expands poleward forming the auroral bulge, which has imbedded flow channels and streamers, and the onset instability extends longitudinally with the continued azimuthal expansion of the bubble within the plasma sheet. The expansion of the bubble is indicated in the observations by a DAPS increase just poleward of the eastward expanding breakup along the growth phase arc, and a SAPS increase just equatorward of the westward expanding breakup along the arc.

The above analysis was considered in the context of an azimuthal expanding bubble as modeled by Wang et al. (2018), and the features we have found are consistent with those from the model as illustrated in Figure 1. Note that the goal of Wang and coworkers was to evaluate and understand bubble evolution, with consideration of substorms, since bubbles are common within the plasma sheet. In addition, the features in the lower panel of Figure 8 are remarkably similar to the features in the schematic summary plot of S. Zou et al. (2009) for the electrodynamics of substorms obtained using the PFISR radar. However, the Zou et al paper was completed prior to the Y. Nishimura et al. (2010b) proposal that a preonset bubble can lead to substorm onset and prior to auroral beading being viewed as a signature of a substorm onset instability. Our analysis indicates that the above very different analyses can all be brought together to form a consistent
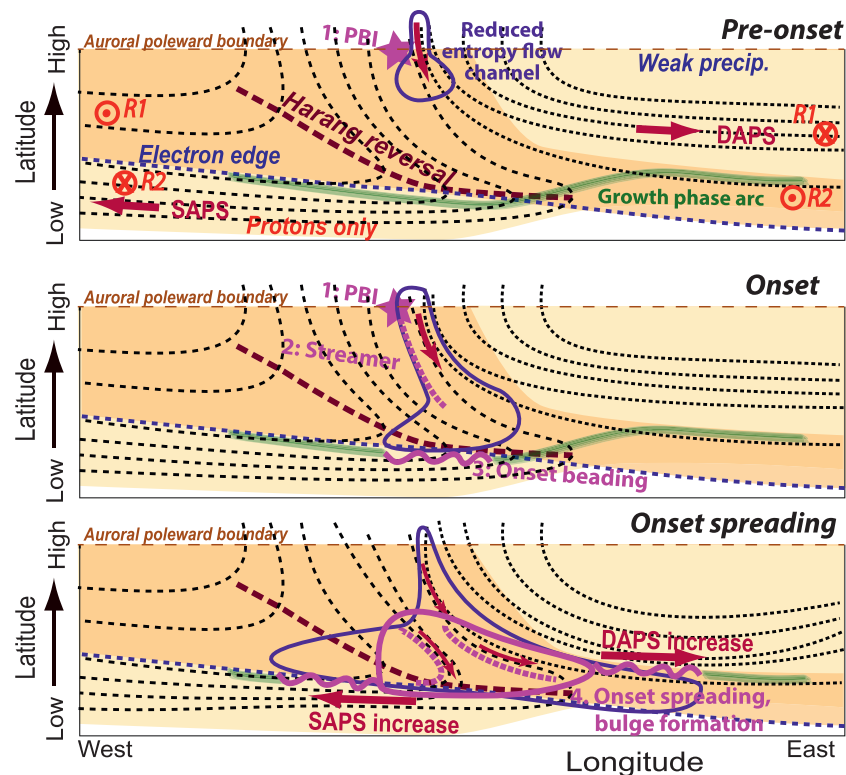
Figure 8. Schematic summary of the substorm onset sequence indicted from the observations in the present and past observation papers, and the RCM-UCLA simulations of Wang et al. (2018). The background convection (dotted and dashed lines) is based on the earlier RCM-UCLA simulations of large-scale convection of Gkioulidou et al. (2009). RCM, Rice Convection Model.

picture of substorm onset via an intruding low entropy flow channels and the azimuthal evolution of the instability. For four our six events, the observations indicated that the azimuthal expansion of the instability was from the azimuthal expansion of the bubble that led to onset. For the other two events, it could have been from the onset bubble or from an early expansion phase bubble. While not directly considered here, it is plausible that azimuthal expansion of bubbles associated with early expansion phase streamers could also contribute to the azimuthal expansion of the instability.

Our observations show an additional interesting feature of substorm westward expansion that is not directly related to the onset instability. As the bulge expands poleward toward the auroral poleward boundary and likely enters the preexisting polar cap, a westward traveling surge can form as observed during the events in Figures 6 and 7. As seem previously by Lyons et al. (2013), the surge appears to slide westward along an arc along or adjacent to the auroral poleward boundary. This poleward boundary arc tilts equatorward as the surge approaches. For what we believe is the first time, we see strong flows adjacent to this arc that appear to bring reduced entropy plasma toward the head of the surge. As clearly seen in the example in Figure 6, this flow channel is not the flow channel that leads to the substorm onset instability but is a feature of the ensuing expansion phase activity. Based on the example in Figure 7, this flow may come from deep in the polar cap, raising the questions of whether the flow brings polar cap plasma along open lobe field lines into the magnetospheric counterpart of the surge. We speculate that the incoming low entropy plasma, whether it is directly from the open polar cap field or from within the distant plasma sheet, may play an important role in the intense activity of the westward traveling surge.

We speculate that the incoming low entropy flow channel contributes to the onset instability by reducing the outward radial gradient of flux tube integrated entropy, and that the azimuthal expansion of the instability is related to the azimuthal expansion of that gradient reduction that occurs as the bubble expands. We do not speculate on what conditions are necessary for an incoming low entropy flow channel to lead to

the substorm onset instability in the inner plasma sheet other than for the necessity of a preceding growth phase, nor do we speculate on what conditions are necessary for a westward traveling surge to form. However, we believe that the observations here are critical to understanding of what triggers substorm onset and its longitudinal expansion, and to what maintains a westward traveling surge and its strong precipitation and currents. We note that, while the observations presented here are consistent with the expansion of a bubble in the plasma sheet, it would be desirable to pursue in situ observations of such expansion from a fortuitous 2 or more spacecraft conjunction event within the inner plasma sheet.

Data Availability Statement

The data we have used here are from THEMIS, CARISMA (Mann et al., 2008), the University of Alaska, and USGS (https://www.usgs.gov/natural-hazards/geomagnetism/science/observatories?qt-science_center_objects=0#qt-science_center_objects). The University of Alaska ASI data are available from http://optics.gi.alaska.edu/optics/, and the THEMIS ASU data from http://themis.ssl.berkeley.edu/themisdata/. The PFISR data are available at amisr.com/database and isr.sri.com/madrigal. All data are properly cited and referred to in the reference list or in the acknowledgments.

References

Birn, J., Raeder, J., Wang, Y. L., Wolf, R. A., & Hesse, M. (2004). On the propagation of bubbles in the geomagnetic tail. *Annales Geophysicae*, *22*(5), 1773–1786. https://doi.org/10.5194/angeo-22-1773-2004

Donovan, E. F., Mende, S., Jackel, B., Syrjäsuo, M., Meurant, M., Voronkov, I., et al. (2006). The azimuthal evolution of the substorm expansive phase onset aurora. In M. Syrjäsuo & E. Donovan (Eds.), *Proceedings of International Conference on Substorms-8* (pp. 55–60). Alberta, Canada: University of Calgary.

Gallardo-Lacourt, B., Nishimura, Y., Lyons, L. R., Mishin, E. V., Ruohoniemi, J. M., Donovan, E. F., et al. (2017). Influence of Auroral Streamers on Rapid Evolution of Ionospheric SAPS Flows. *Journal of Geophysical Research: Space Physics*, *122*(12), 12406–12420. https://doi.org/10.1002/2017JA024198

Gkioulidou, M., Wang, C.-P., & Lyons, L. R. (2011). Effect of self-consistent magnetic field on plasma sheet penetration to the inner magnetosphere: Rice convection model simulations combined with modified Dungey force-balanced magnetic field solver. *Journal of Geophysical Research*, *116*(A12), A12213. https://doi.org/10.1029/2011JA016810

Gkioulidou, M., Wang, C.-P., Lyons, L. R., & Wolf, R. A. (2009). Formation of the Harang reversal and its dependence on plasma sheet conditions: Rice convection model simulations. *Journal of Geophysical Research*, *114*(A7), A07204. https://doi.org/10.1029/2008JA013955

Gkioulidou, M., Wang, C.-P., Wing, S., Lyons, L. R., Wolf, R. A., & Hsu, T.-S. (2012). Effect of an MLT dependent electron loss rate on the magnetosphere-ionosphere coupling. *Journal of Geophysical Research*, *117*(A11), A11218. https://doi.org/10.1029/2012JA018032

Haerendel, G. (2015). Substorm onset: Current sheet avalanche and stop layer. *Journal of Geophysical Research: Space Physics*, *120*(3), 1697–1714. https://doi.org/10.1002/2014JA020571

Heinselman, C. J., & Nicolls, M. J. (2008). A Bayesian approach to electric field and *E*-region neutral wind estimation with the Poker Flat Advanced Modular Incoherent Scatter Radar. *Radio Science*, *43*(5), RS5013. https://doi.org/10.1029/2007RS003805

Henderson, M. G., Kepko, L., Spence, H. E., Connors, M., Sigwarth, J. B., Frank, L. A., & singer, H. J. (2002). The evolution of north-south aligned auroral forms into auroral torch structures: The generation of omega bands and ps6 pulsations via flow bursts. In R. M. Winglee (Ed.), *Sixth International Conference on Substorms* (pp. 169–174). Seattle: The University of Washington.

Henderson, M. G., Reeves, G. D., & Murphree, J. S. (1998). Are north-south aligned auroral structures an ionospheric manifestation of bursty bulk flows? *Geophysical Research Letters*, *25*(19), 3737–3740.

Kalmoni, N. M. E., Rae, I. J., Murphy, K. R., Forsyth, C., Watt, C. E. J., & Owen, C. J. (2017). Statistical azimuthal structuring of the substorm onset arc: Implications for the onset mechanism. *Geophysical Research Letters*, *44*(5), 2078–2087. https://doi.org/10.1002/2016GL071826

Liu, J., Angelopoulos, V., Chu, X., Zhou, X.-Z., & Yue, C. (2015). Substorm current wedge composition by wedgelets. *Geophysical Research Letters*, *42*(6), 1669–1676. https://doi.org/10.1002/2015GL063289

Liu, J., Lyons, L. R., Archer, W. E., Gallardo-Lacourt, B., Nishimura, Y., Zou, Y., et al. (2018). Flow shears at the poleward boundary of omega bands observed during conjunctions of swarm and THEMIS ASI. *Geophysical Research Letters*, *45*(3), 1218–1227. https://doi.org/10.1002/2017GL076485

Liu, J., Lyons, L. R., Wang, C.-P., Hairston, M. R., Zhang, Y., & Zou, Y. (2020). Dawnside auroral polarization streams. *Journal of Geophysical Research: Space Physics*, *125*(8), http://dx.doi.org/10.1029/2019ja027742

Lyons, L. R., & Fennell, J. F. (1986). Characteristics of auroral electron precipitation on the morningside. *Journal of Geophysical Research*, *91*(A10), 11225–11234. https://doi.org/10.1029/JA091iA10p11225

Lyons, L. R., Liu, J., Nishimura, Y., Reimer, A. S., Bristow, W. A., Hampton, D. L., et al. (2021). Radar observations of flows leading to substorm onset over Alaska. *Journal of Geophysical Research: Space Physics*, *126*, e2020JA028147. https://doi.org/10.1029/2020JA028147.

Lyons, L. R., Nishimura, Y., Gallardo-Lacourt, B., Nicolls, M. J., Chen, S., Hampton, D. L., et al. (2015). Azimuthal flow bursts in the inner plasma sheet and possible connection with SAPS and plasma sheet earthward flow bursts. *Journal of Geophysical Research: Space Physics*, *120*(6), 5009–5021, 2015JA021023. https://doi.org/10.1002/2015JA021023

Lyons, L. R., Nishimura, Y., Gallardo-Lacourt, B., Zou, Y., Donovan, E., Mende, S., et al. (2013). Westward traveling surges: Sliding along boundary arcs and distinction from onset arc brightening. *Journal of Geophysical Research: Space Physics*, *118*(12), 7643–7653. https://doi.org/10.1002/2013JA019334

Lyons, L. R., Nishimura, Y., Xing, X., Runov, A., Angelopoulos, V., Donovan, E., & Kikuchi, T. (2012). Coupling of dipolarization front flow bursts to substorm expansion phase phenomena within the magnetosphere and ionosphere. *Journal of Geophysical Research: Space Physics*, *117*(A2). http://dx.doi.org/10.1029/2011ja017265

Makarevich, R. A., & Bristow, W. A. (2014). Coordinated radar observations of plasma wave characteristics in the auroral F region. *Annales Geophysicae*, *32*(7), 875–888. https://doi.org/10.5194/angeo-32-875-2014

Makarevich, R. A., Kellerman, A. C., Devlin, J. C., Ye, H., Lyons, L. R., & Nishimura, Y. (2011). SAPS intensification during substorm recovery: A multi-instrument case study. *Journal of Geophysical Research: Space Physics*, *116*(A11). http://dx.doi.org/10.1029/2011ja016916

Mann, I. R., Milling, D. K., Rae, I. J., Ozeke, L. G., Kale, A., Kale, Z. C., et al. (2008). The upgraded CARISMA magnetometer array in the THEMIS era. *Space Science Reviews*, *141*(1–4), 413–451. https://doi.org/10.1007/s11214-008-9457-6

Motoba, T., Hosokawa, K., Kadokura, A., & Sato, N. (2012). Magnetic conjugacy of northern and southern auroral beads. *Geophysical Research Letters*, *39*(8). http://dx.doi.org/10.1029/2012gl051599

Nishimura, Y., Lyons, L. R., Kikuchi, T., Angelopoulos, V., Donovan, E., Mende, S., et al. (2012). Formation of substorm Pi2: A coherent response to auroral streamers and currents. *Journal of Geophysical Research: Space Physics*, *117*(A9). http://dx.doi.org/10.1029/2012ja017889

Nishimura, Y., Lyons, L., Zou, S., Angelopoulos, V., & Mende, S. (2010). Substorm triggering by new plasma intrusion: THEMIS all-sky imager observations. *Journal of Geophysical Research: Space Physics*, *115*(A7). http://dx.doi.org/10.1029/2009ja015166

Nishimura, Y., Lyons, L. R., Zou, S., Angelopoulos, V., & Mende, S. B. (2010). Reply to comment by Harald U. Frey on "Substorm triggering by new plasma intrusion: THEMIS all-sky imager observations". *Journal of Geophysical Research: Space Physics*, *115*(A12). http://dx.doi.org/10.1029/2010ja016182

Nishimura, Y., Yang, J., Pritchett, P. L., Coroniti, F. V., Donovan, E. F., Lyons, L. R., et al. (2016). Statistical properties of substorm auroral onset beads/rays. *Journal of Geophysical Research: Space Physics*, *121*(9), 8661–8676. https://doi.org/10.1002/2016JA022801

Ogasawara, K., Kasaba, Y., Nishimura, Y., Hori, T., Takada, T., Miyashita, Y., et al. (2011). Azimuthal auroral expansion associated with fast flows in the near-Earth plasma sheet: Coordinated observations of the THEMIS all-sky imagers and multiple spacecraft. *Journal of Geophysical Research: Space Physics*, *116*(A6). http://dx.doi.org/10.1029/2010ja016032

Sakaguchi, K., Shiokawa, K., Ieda, A., Nomura, R., Nakajima, A., Greffen, M., et al. (2009). Fine structures and dynamics in auroral initial brightening at substorm onsets. *Annales Geophysicae*, *27*(2), 623–630. https://doi.org/10.5194/angeo-27-623-2009

Shiokawa, K., Ieda, A., Nakajima, A., Sakaguchi, K., Nomura, R., Aslaksen, T., et al. (2009). Longitudinal development of a substorm brightening arc. *Annales Geophysicae*, *27*(5), 1935–1940. https://doi.org/10.5194/angeo-27-1935-2009

Wang, C.-P., Gkioulidou, M., Lyons, L. R., & Wolf, R. A. (2018). Spatial Distribution of Plasma Sheet Entropy Reduction Caused by a Plasma Bubble: Rice Convection Model Simulations. *Journal of Geophysical Research: Space Physics*, *123*(5), 3380–3397. https://doi.org/10.1029/2018JA025347

Wang, C.-P., Gkioulidou, M., Lyons, L. R., Wolf, R. A., Angelopoulos, V., Nagai, T., et al. (2011). Spatial distributions of ions and electrons from the plasma sheet to the inner magnetosphere: Comparisons between THEMIS-Geotail statistical results and the Rice Convection Model. *Journal of Geophysical Research*, *116*, A11216. https://doi.org/10.1029/2011JA016809

Xing, X., & Wolf, R. A. (2007). Criterion for interchange instability in a plasma connected to a conducting ionosphere. *Journal of Geophysical Research: Space Physics*, *112*(A12), A12209. https://doi.org/10.1029/2007JA012535

Yang, J., Toffoletto, F. R., & Wolf, R. A. (2014). RCM-E simulation of a thin arc preceded by a north-south-aligned auroral streamer. *Geophysical Research Letters*, *41*(8), 2695–2701. https://doi.org/10.1002/2014GL059840

Zhang, X.-J., Angelopoulos, V., Runov, A., Zhou, X.-Z., Bonnell, J., McFadden, J. P., et al. (2011). Current carriers near dipolarization fronts in the magnetotail: A THEMIS event study. *Journal of Geophysical Research: Space Physics*, *116*(A5). http://dx.doi.org/10.1029/2010ja015885

Zou, S., Lyons, L. R., Nicolls, M. J., Heinselman, C. J., & Mende, S. B. (2009). Nightside ionospheric electrodynamics associated with substorms: PFISR and THEMIS ASI observations. *Journal of Geophysical Research: Space Physics*, *114*(A12). http://dx.doi.org/10.1029/2009ja014259

Zou, Y., Nishimura, Y., Lyons, L. R., Shiokawa, K., Donovan, E. F., Ruohoniemi, J. M., et al. (2015). Localized polar cap flow enhancement tracing using airglow patches: Statistical properties, IMF dependence, and contribution to polar cap convection. *Journal of Geophysical Research: Space Physics*, *120*(5), 4064–4078. https://doi.org/10.1002/2014JA020946